ELSEVIER

Journal of Organometallic Chemistry 565 (1998) 193–200

Journal of Organometallic Chemistry

High nuclearity ruthenium carbonyl cluster chemistry VII[1]. Synthesis, NMR studies, electrochemistry and X-ray crystal structure of [PPN] $[Ru_8(\mu_8\text{-P})(CO)_{22}]$[2]

Marie P. Cifuentes [a,*], Susan M. Waterman [a], Mark G. Humphrey [a], Graham A. Heath [b], Brian W. Skelton [c], Allan H. White [c], M.P. Seneka Perera [d], Michael L. Williams [d]

[a] *Department of Chemistry, Australian National University, Canberra, ACT 0200, Australia*
[b] *Research School of Chemistry, Australian National University, Canberra. ACT 0200, Australia*
[c] *Department of Chemistry, University of Western Australia, Nedlands, WA 6907, Australia*
[d] *Faculty of Science & Technology, Griffith University, Nathan Campus, Brisbane, Qld 4111, Australia*

Received 12 December 1997

Abstract

The reaction between $[Ru_3(\mu\text{-H})(\mu\text{-NC}_5H_4)(CO)_{10}]$ and chlorodiphenylphosphine in refluxing chlorobenzene, followed by metathesis with bis(triphenylphosphoranylidene)ammonium chloride ([PPN]Cl), affords $[PPN][Ru_8(\mu_8\text{-P})(CO)_{22}]$ (**1**) in around 30% yield. ^{31}P-NMR solution spectra are consistent with the presence of at least two isomers of the cluster anion, presumably due to differing carbonyl distributions; the chemical shifts for these configurations (600–800 ppm downfield of H_3PO_4) are consistent with a highly deshielded interstitial phosphorus atom. An X-ray structural study of one isomer of **1** reveals that the phosphorus atom occupies an interstitial square antiprismatic site defined by the eight ruthenium atoms, with two bridging carbonyl ligands on opposite faces spanning interplanar Ru–Ru bonds, and twenty terminal carbonyl ligands completing the ligand set. The solid state ^{31}P-NMR spectrum of the crystallographically-identified isomer reveals a signal at 596.1 ppm assigned to the square antiprismatic interstitial phosphorus atom. Formal electron counting suggests that **1** has four electrons less than expected using Wade's rules. The reductive electrochemistry of **1** has been examined by cyclic voltammetry, and reveals the presence of two one-electron and one two-electron reduction waves, an uptake of four electrons in total, consistent with the cluster's theoretical electron deficiency in the resting state.

Keywords: Interstitial phosphido; Ruthenium cluster; Square antiprism; ^{31}P solid state NMR; X-ray structure; Voltammetry

1. Introduction

High-nuclearity (M_n, $n \geq 7$) metal clusters are of interest as intermediates in the transition from molecular to metallic behaviour [2,3], but investigations into their chemistry have often been frustrated by the lack of useful preparative routes into such clusters [4]. High-nuclearity group 8 carbonyl clusters are still comparitively rare, with bridge-assisted and condensation reactions being the principal synthetic methods employed. Many examples of high-nuclearity clusters containing interstitial atoms such as hydrogen or first row elements (e.g. carbon, boron and nitrogen) exist, but analogues with heavier elements in the interstices are rarer. For the latter, bridge-assisted cluster synthesis using sulfur- and phosphorus-containing ligands has been the most successful route, with the P-ligands affording high-nuclearity clusters with phosphine residues

* Corresponding author. Tel.: +61 2 62494293; fax: +61 2 62490760; e-mail: Marie.Cifuentes@anu.edu.au

[1] For Part VI, see Ref. [1].

[2] Dedicated to Professor Michael I. Bruce on the occasion of his 60th birthday. MPC thanks MIB for sparking her interest in cluster chemistry.

0022-328X/98/$19.00
PII S0022-328X(98)00452-5

Table 1
^{31}P-NMR shifts (ppm)[a] for some interstitial phosphido ligands in medium- and high-nuclearity (M_n, $n \geq 6$) carbonyl clusters

Complex	δ^{31}P	Cluster geometry	Ref.
$[Fe_3(\mu\text{-H})_2(\mu_6\text{-P})(CO)_9\{Au(PPh_3\}_3]$[b]	265.2	External edge-bridged bow-tie	[13]
$[Co_6(\mu_6\text{-P})(CO)_{16}]^-$[b]	486.2[c]	Two edge-fused butterflies	[14]
$[Os_6(\mu\text{-H})(\mu_6\text{-P})(CO)_{18}]$	607.9	Trigonal prism	[15,16]
$[Os_6(\mu_6\text{-P})(CO)_{18}]^-$	662.4	Trigonal prism	[15,16]
$[Os_6(\mu_3\text{-AuPPh}_3)(\mu_6\text{-P})(CO)_{18}]$	638.4	Capped trigonal prism	[15]
$[Ru_6(\mu\text{-H})_6(\mu_6\text{-P})(\mu\text{-PHBu}^n)(\mu\text{-PBu}^n_2)_2(PBu^n_3)_2(CO)_{10}]$[b]	88.7	External edge-bridged bow-tie	[17]
$[Ru_6(\mu\text{-H})_6(\mu_6\text{-P})(\mu\text{-PBu}^n_2)(PBu^n_3)_2(CO)_{13}]$[b]	204.3	Square based boat	[18]
$[Ru_8(\mu_6\text{-P})(\mu_4\text{-PPh})(\mu\text{-PPh}_2)(CO)_{22}]$[b]	554.4	Scorpion fused to basal edge of a square pyramid	[19]
$[Ru_8(\mu_8\text{-P})(CO)_{22}]^-$	620.4, 774.8	Square antiprism	This work
$[Rh_9(\mu_8\text{-P})(CO)_{21}]^{2-}$	282.3	Capped square antiprism	[20]
$[Rh_{10}(\mu_8\text{-P})(CO)_{22}]^{3-}$	369.3	Bicapped square antiprism	[21]

[a] Referenced relative to external H_3PO_4.
[b] (μ_6-P) is in a semi-encapsulated site.
[c] 190 K.

in environments ranging from edge-bridging to μ_8-encapsulated P atoms [4].

We have previously reported the synthesis of the decaruthenium anion $[Ru_{10}(\mu\text{-H})(\mu_6\text{-C})(CO)_{24}]^-$ via the thermolysis of $[Ru_3(\mu\text{-H})(\mu\text{-NC}_5H_4)(CO)_{10}]$ in chlorobenzene [5–7], and have been investigating its reactivity towards nucleophiles such as triphenylphosphine and trimethylphosphite [6–9], as well as probing its electronic and magnetic properties [10] and reductive electrochemistry [1]. As part of ongoing investigations into the thermolysis reactions of $[Ru_3(\mu\text{-H})(\mu\text{-NC}_5H_4)(CO)_{10}]$ we report below its reaction with $PClPh_2$ in refluxing chlorobenzene to give the octanuclear phosphido cluster $[PPN][Ru_8(\mu_8\text{-P})(CO)_{22}]$ [PPN = bis(triphenylphosphoranylidene)ammonium] (**1**), including an X-ray structural study of one isomeric configuration of **1** and results from our initial studies into its reductive electrochemistry.

2. Results and discussion

2.1. Syntheses and characterization of $[PPN][Ru_8(\mu_8\text{-P})(CO)_{22}]$

The reaction between $[Ru_3(\mu\text{-H})(\mu\text{-NC}_5H_4)(CO)_{10}]$ and $PClPh_2$ in refluxing chlorobenzene over 40 min, followed by stirring with [PPN]Cl and purification by thin layer chromatography, afforded a number of bands. The major product, obtained in ca. 20–30% yield, was identified as $[PPN][Ru_8(\mu_8\text{-P})(CO)_{22}]$ (**1**) by a combination of FAB mass spectrometry, IR-, ^{1}H-, ^{13}C- and ^{31}P-NMR spectroscopies, satisfactory microanalyses and a single crystal X-ray diffraction study. The solution IR spectrum contains ν(CO) bands assigned to terminal carbonyl ligands at 2049 (s), 2024 (m) and 1985 (w) cm^{-1}, as well as a weak band at 1790 cm^{-1} assigned to bridging CO groups. The negative ion FAB mass spectrum contains a signal at m/z 1456 corresponding to the parent ion $[Ru_8(\mu_8\text{-P})(CO)_{22}]^-$, as well as peaks due to successive loss of up to 15 CO units. Signals for the $[PPN]^+$ cation are found in the appropriate regions of the ^{1}H- and ^{13}C-NMR spectra; no evidence was found for the presence of metal-bound hydrides in the proton NMR spectrum. Resonances due to the carbonyl ligands occur as a set of closely spaced, unresolved signals centred at 202.8 and a sharp signal at 201.7 ppm, in the ratio of ca. 10:1, and a second very broad set of signals of indeterminate integral at around 196.5–191 ppm; signals corresponding to bridging CO ligands are not seen. As the broad signals may result from interconverting structural isomers, attempts were made to resolve the putative fluxionality. Lowering the temperature to 183 K results in replacement of the signals at 202.8 by a broad singlet at 202.0 ppm, with the resonance at 201.7 ppm remaining a sharp singlet; little change is observed in the set of broad resonances. The ^{31}P-NMR spectrum is also complex. The CD_2Cl_2 spectrum at 298 K contains a resonance due to the $[PPN]^+$ cation (21.5 ppm) together with low field resonances assigned to an interstitial phosphorus atom at 620.4 and 774.8 ppm, with a relative integral of 15:6.5:1, respectively, a ratio consistent with the proposed formulation. A similar spectrum at 298 K using d_6-acetone as solvent reveals a broadened resonance at 619.5 ppm, with the other two signals remaining sharp. No additional clarification was obtained on running the spectrum of **1** in d_6-acetone at 213 K.

The carbon- and phosphorus-solution NMR spectra are thus suggestive of the presence of structural isomers—two in CD_2Cl_2 solution, and possibly more than this in d_6-acetone—with these isomers interconverting by fluxional pathways. In order to resolve the nature of the signals observed in the phosphorus-NMR spectra, solid state ^{31}P-NMR spectra was obtained from a sample crystallized under the same conditions as the sample

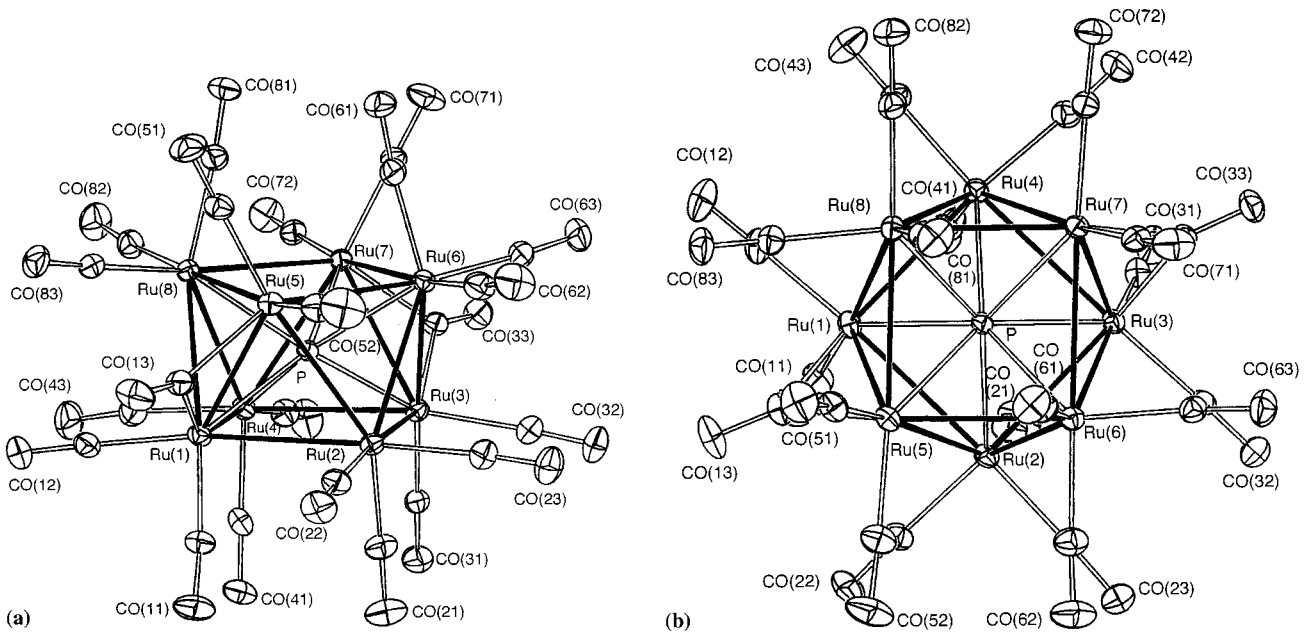

Fig. 1. Thermal ellipsoid diagrams of the $[Ru_8(\mu_8\text{-P})(\mu\text{-CO})_2(CO)_{20}]^-$ anion; ellipsoids show 20% probability levels.

for the structural study (see below). A spectrum with a pulse delay of 10 s shows two signals in the ration of 1:1 at 6.7 and 9.8 ppm, assigned to the $[PPN]^+$ cation, and consistent with the structural study below which reveals that the phosphorus atoms in the cation are not symmetry related in the crystal lattice. More interestingly, a spectrum with a pulse delay of 900 s shows a signal at 596.1 ppm, assigned to the μ_8-P interstitial phosphorus in the crystallographically identified configuration. The NMR data are thus consistent with the presence of at least three configurations in solution, which possibly vary due to differing carbonyl distributions.

Table 2
Selected bond lengths (A) for **la**

Ru–Ru bonds			
Ru(l)–Ru(2)	2.9644(8)	Ru(l)–Ru(5)	2.8285(7)
Ru(l)–Ru(4)	2.8984(8)	Ru(l)–Ru(8)	2.945(1)
Ru(2)–Ru(3)	2.9142(8)	Ru(2)–Ru(5)	2.9250(8)
Ru(3)–Ru(4)	2.9724(8)	Ru(2)–Ru(6)	2.8918(9)
Ru(5)–Ru(6)	2.9373(7)	RU(3)–Ru(6)	2.938(1)
Ru(5)–Ru(8)	2.9599(7)	Ru(3)–Ru(7)	2.8137(8)
Ru(6)–Ru(7)	2.9791(7)	Ru(4)–Ru(7)	2.9217(7)
Ru(7)–Ru(8)	2.9486(7)	Ru(4)–Ru(8)	2.894(1)
Ru–Phosphido bonds			
Ru(l)–P	2.421(1)	Ru(5)–P	2.415(1)
Ru(2)–P	2.407(1)	Ru(6)–P	2.392(1)
Ru(3)–P	2.412(1)	Ru(7)–P	2.414(1)
Ru(4)–P	2.404(1)	Ru(8)–P	2.398(1)
Ru–C			
Ru(1)–C(13)	2.070(5)	Ru(3)–C(33)	2.069(4)
Ru(5)–C(13)	2.051(5)	Ru(7)–C(33)	2.083(4)
Ru–terminal C: range 1.864(4)–1.934(5) Å, average 1.895 Å			

T_1 measurements on the 775 and 620 ppm signals using the inversion recovery procedure revealed spin-lattice relaxation times of 20.8 ± 8.3 and 14.0 ± 8.5 s, respectively, the first such data for interstitial phosphorus atoms. T_1 data for interstitial carbon and nitrogen atoms in octahedral, trigonal prismatic and square antiprismatic sites in carbonyl clusters have been dis-

Table 3
Metal cluster core angles (°) for **1a**

Bond angles	(°)		(°)
Ru(2)–Ru(1)–Ru(4)	89.05(2)	Ru(1)–Ru(5)–Ru(6)	103.26(3)
Ru(2)–Ru(l)–Ru(5)	60.60(2)	Ru(l)–Ru(5)–Ru(8)	61.11(2)
Ru(2)–Ru(l)–Ru(8)	101.26(2)	Ru(2)–Ru(5)–Ru(6)	59.11(2)
Ru(4)–Ru(l)–Ru(5)	103.89(3)	Ru(2)–Ru(5)–Ru(8)	101.84(3)
Ru(4)–Ru(l)–Ru(8)	59.37(2)	Ru(6)–Ru(5)–Ru(8)	88.08(2)
Ru(5)–Ru(l)–Ru(8)	61.65(2)	Ru(2)–Ru(6)–Ru(3)	59.98(1)
Ru(l)–Ru(2)–Ru(3)	91.07(2)	Ru(2)–Ru(6)–Ru(5)	60.23(2)
Ru(l)–Ru(2)–Ru(5)	57.40(2)	Ru(2)–Ru(6)–Ru(7)	100.71(2)
Ru(1)–Ru(2)–Ru(6)	101.06(2)	Ru(3)–Ru(6)–Ru(5)	101.94(2)
Ru(3)–Ru(2)–Ru(5)	102.81(3)	Ru(3)–Ru(6)–Ru(7)	56.79(2)
Ru(3)–Ru(2)–Ru(6)	60.79(2)	Ru(5)–Ru(6)–Ru(7)	92.00(2)
Ru(5)–Ru(2)–Ru(6)	60.66(2)	Ru(3)–Ru(7)–Ru(4)	62.40(2)
Ru(2)–Ru(3)–Ru(4)	88.59(2)	Ru(3)–Ru(7)–Ru(6)	60.86(2)
Ru(2)–Ru(3)–Ru(6)	59.23(2)	Ru(3)–Ru(7)–Ru(8)	103.37(2)
Ru(2)–Ru(3)–Ru(7)	104.23(2)	Ru(4)–Ru(7)–Ru(6)	101.51(2)
Ru(4)–Ru(3)–Ru(7)	60.58(2)	Ru(4)–Ru(7)–Ru(8)	59.07(2)
Ru(6)–Ru(3)–Ru(7)	62.35(2)	Ru(6)–Ru(7)–Ru(8)	87.51(2)
Ru(l)–Ru(4)–Ru(3)	91.22(2)	Ru(l)–Ru(8)–Ru(4)	59.92(2)
Ru(l)–Ru(4)–Ru(7)	103.40(2)	Ru(l)–Ru(8)–Ru(5)	57.25(2)
Ru(l)–Ru(4)–Ru(8)	61.11(2)	Ru(l)–Ru(8)–Ru(7)	101.62(2)
Ru(3)–Ru(4)–Ru(7)	57.02(2)	Ru(4)–Ru(8)–Ru(5)	100.77(2)
Ru(3)–Ru(4)–Ru(8)	100.86(2)	Ru(4)–Ru(8)–Ru(7)	60.00(2)
Ru(7)–Ru(4)–Ru(8)	60.93(2)	Ru(5)–Ru(8)–Ru(7)	92.16(2)
Ru(l)–Ru(5)–Ru(2)	62.00(2)		

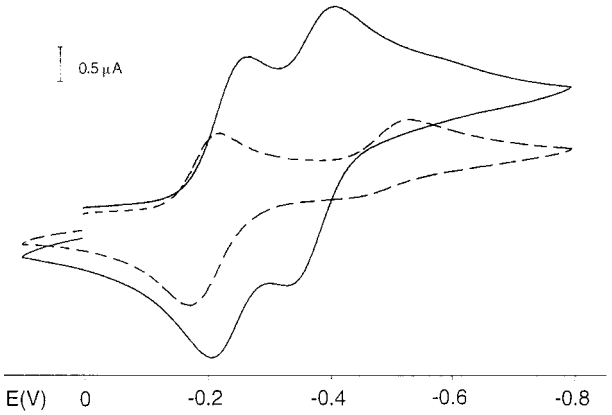

Fig. 2. Cyclic voltammogram of **1** at 223 (dashed line), 298 K.

cussed recently by Heaton et al. [11], with the major relaxation pathways for the cobalt, rhodium and nickel cluster examples being dependent on shielding anisotropy and dipole–dipole interactions. In the absence of T_1 data for other representative examples of clusters with interstitial phosphorus, it is difficult to be certain of the relative importance of the possible relaxation pathways in the present cluster. Heaton et al. found that the square antiprismatic nickel carbido clusters had very long T_1 values, indicating smaller shielding anisotropy, and a closer approach to sp^3 hybridization of the interstitial carbon in the square antiprismatic site (they propose the carbon to be ca. sp^2 hybridized in trigonal prismatic sites, and sp hybridized in octahedral interstices). It has subsequently been pointed out, though, that hybridization concepts are not appropriate in strongly delocalized systems, although the close relationship between shielding anisotropy and the detailed structure of the cluster cavity was confirmed [12]. The expectation with the present cluster, which has an almost idealized square antiprismatic core geometry,

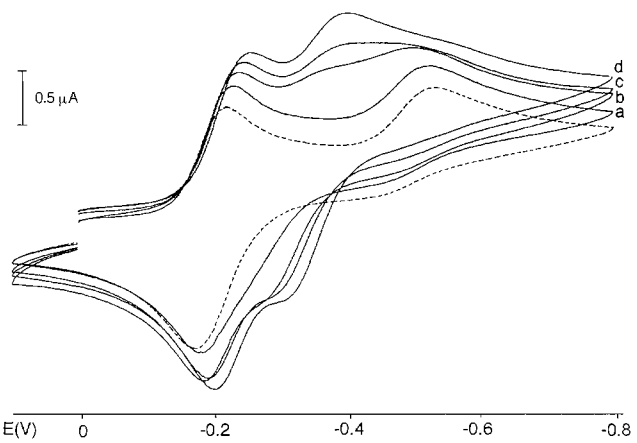

Fig. 3. Cyclic voltammogram of **1** showing the effect of increasing the temperature from 223 K (dashed line) through (a) 238; (b) 248; (c) 258; to (d) 268 K.

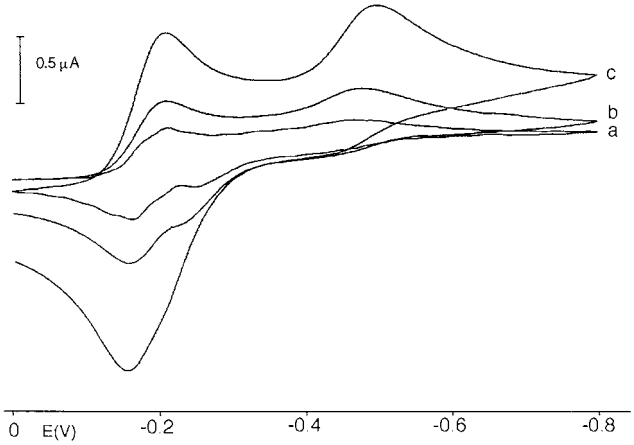

Fig. 4. Cyclic voltammogram of **1** at 223 K showing the effect of varying the scan rate from 10 (a) through 25 (b) to 100 (c) mV s^{-1}.

would be for a long T_1 value due to decreased shielding anisotropy—further data are required to confirm this.

^{31}P-NMR data for crystallographically-verified interstitial phosphorus ligands in carbonyl clusters are collected in Table 1. The resonance at 775 ppm corresponds to the most deshielded interstitial phosphide thus far. Mason has correlated deshielding with compression of interstitial atoms in cluster carbides, nitrides [22] and borides [23]. The phosphorus nuclei in metal phosphides with infinite solid state structures have chemical shifts in the range -6 to -262 ppm (i.e. highly shielded with respect to cluster-bound interstitial phosphides). At present, there is no interpretation of the factors influencing ^{31}P chemical shifts in cluster phosphides [24], but it seems logical that the deshielding-interstitial atom compression idea which has been successfully applied to cluster carbides, nitrides and borides should have applicability to phosphides. The crystallographically identified isomer has two bridging carbonyls (see below) with an isotropic solid state ^{31}P

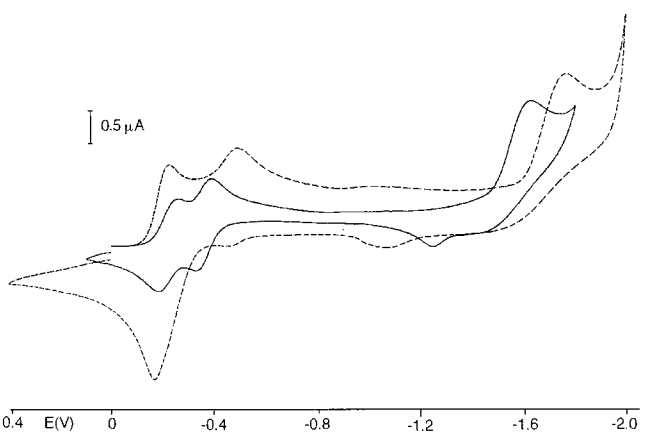

Fig. 5. Cyclic voltammogram of **1** at 223 (dashed line) and 298 K using a switching potential of -1.80 to -2.00 V.

Table 4
Summary of the cyclic voltammetric data for **1** (vs Ag/AgCl)

Temperature (K)	E_p^c (V)	E_p^a (V)	E^0 (V)
298	−0.27	−0.21	−0.24
	−0.40	−0.34	−0.37
	−1.63	−1.25	−1.44
223	−0.22	−0.17	−0.20
	−0.53	−0.44	−0.49
	−1.76	−1.07	−1.42

chemical shift of 596.1 ppm. It is possible, then, that the signal at 774.8 ppm in the solution ^{31}P-NMR spectrum corresponds to an isomer with a different number of bridging carbonyls, and consequently different average Ru–Ru bond lengths and decreased cavity size, but further speculation is not warranted; the theory that interstitial cavity compression necessarily results in deshielding has been questioned recently [12].

2.2. X-ray structure of [PPN][$Ru_8(\mu_8$-P)(μ-CO)$_2$(CO)$_{20}$] (**1a**)

The identity of **1** was confirmed by an X-ray crystal structure study of one of its isomers. An ORTEP plot of the anion of **1a** is shown in Fig. 1, and selected bond lengths and angles are displayed in Tables 2 and 3, respectively. The title complex is only the second structurally characterized example of an octametallic cluster with an interstitial μ_8-phosphido ligand, and the first to be obtained in useful yields. The only precedent, [$Ru_8(\mu_8$-P)(μ-η,η^6-CH_2Ph)(μ-CO)$_2$(CO)$_{17}$] (**2**), was observed 'intermittently' in less than 2% yield as the 14th band following chromatography from the reaction of [Ru_3(CO)$_{12}$] with $PHPh_2$, and characterized by X-ray crystallography only [25,26]. Interestingly, we have found that reaction between [$Ru_3(\mu$-H)(μ-NC_5H_4)(CO)$_{10}$] and $PHPh_2$ in refluxing chlorobenzene gives a large number of bands, from which [$Ru_6(\mu_6$-H)(CO)$_{18}$]$^-$ [27] has been identified as the main product; cluster **1** was obtained in trace amounts only.

The anion of **1a** has eight ruthenium atoms arranged in a square antiprismatic geometry, with a phosphorus atom occupying the interstitial cavity, an arrangement similar to that found for the related **2** [25,26]. Twenty two carbonyl ligands in **1a** are arranged as 20 terminal and two slightly asymmetric bridging groups. The basal square Ru–Ru bond distances [2.8984(8)–2.9971(7) Å, av. 2.9490 Å], non-carbonyl-bridged interplanar Ru–Ru bonds [2.8918(9)–2.945(1) Å, av. 2.919 Å] and the carbonyl-bridged interplanar Ru–Ru vectors [2.8137(8), 2.8285(7) Å, av. 2.8211 Å] are similar to those found for **2** [2.839(5)–2.998(5) Å, av. 2.917 Å; 2.822(5)–3.021(5) Å, av. 2.901 Å; 2.819(5)–2.858(5) Å, av. 2.841 Å], with differences arising from the presence of the η^1,η^6-benzyl ligand in the latter. For **1a**, bridging CO ligands lie on opposite faces of the square antiprism and span the shortest interplanar Ru–Ru bonds. This is in contrast to cluster **2**, where they occur one each on interplanar and basal Ru–Ru bonds associated with the ruthenium atom bearing the σ-linkage to the benzyl group, presumably to alleviate the associated increase in electron density at this metal atom. Terminal Ru–CO distances are 'normal' [1.864(4)–1.934(5) Å, av. 1.895 Å] and the associated Ru–C–O bond angles are approximately linear [$\angle$169.1(5)–178.5(4)°], with differences from linearity probably arising from packing forces. Ruthenium–phosphorus bond distances in **1a** [2.392(1)–2.421(1) Å, av. 2.408 Å] lie within the range found in **2** [2.29(1)–2.44(1) Å, av. 2.39 Å], with the greater asymmetry in the latter due to a displacement of the interstitial phosphido ligand towards the ruthenium bearing the η^6-benzyl interaction. The absence of the organic residue (which is present in **2**) results in cluster **1a** possessing a metal core which is, overall, less distorted from its idealized square antiprismatic geometry. The accompanying $[PPN]^+$ cation is 'normal'; P–N bond distances are 1.571(4), 1.570(4) Å with a P–N–P bond angle of 146.3(3)°, P–C bond lengths range between 1.797(2)–1.804(5) Å, and N–P–C bond angles between 107.2–117.2(2)°.

A square antiprism is an example of an arachno geometry, derived from the parent closo structure, the bicapped square antiprism, by removal of the two caps; application of Wade's rules leads to an expected cluster valence electron count of 118. Formal electron counting reveals that cluster **1** has 114 electrons, i.e. it is four electrons deficient. Cluster **2** was reported to be electron precise [26] but is in fact isoelectronic with **1**, and thus is also four electrons deficient. Only a few other clusters with square antiprismatic core geometry are known and, of these, the rhodium complexes [$Rh_9(\mu_8$-P)(μ-CO)$_{12}$(CO)$_9$]$^{2-}$ [20], [$Rh_{10}(\mu_8$-P)(μ-CO)$_{12}$(CO)$_{10}$]$^{3-}$ [21], [$Rh_{10}(\mu_8$-S)(μ-CO)$_{12}$(CO)$_{10}$]$^{2-}$ [28] and [$Rh_{10}(\mu_8$-As)(μ-CO)$_{12}$(CO)$_{10}$]$^{3-}$ [29] are electron precise. In contrast, [$Co_8(\mu_8$-C)(μ-CO)$_{10}$(CO)$_8$]$^{2-}$ [30,31] is also four electrons deficient and [$Co_9(\mu_8$-Si)(μ-CO)$_8$(CO)$_{13}$]$^{2-}$ [32] is a paramagnetic, one electron deficient cluster.

2.3. Electrochemical studies of **1**

In order to ascertain whether the formal electron deficiency of cluster **1** corresponds to ready reducibility, we have commenced studies of its electrochemical behaviour. Fig. 2 shows the cyclic voltammetric response of a dichloromethane solution of **1** in the range 0.10 to −0.80 V at 298 and 223 K. Two reversible waves (E_0 = −0.24 and −0.37 V) are evident at r.t. with succeeding traces being identical to the first. The scan at 223 K shows that the first reduction step remains virtually unchanged upon lowering the temperature; however, the second wave has shifted to significantly

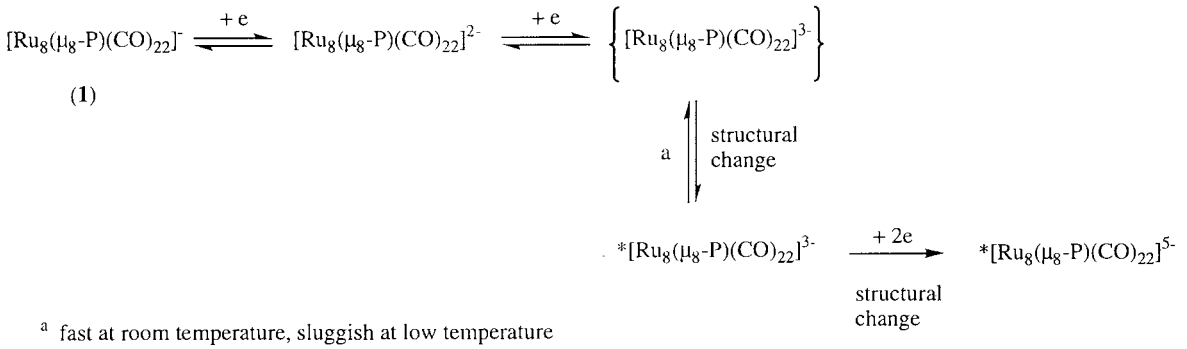

[a] fast at room temperature, sluggish at low temperature

* indicates the structurally altered complex

Scheme 1. Interpretation of electrochemical studies on **1**.

more negative reduction potentials ($E_0 = -0.49$ V) and becomes, in contrast, obviously electrochemically irreversible. Rather than the second reductive peak simply shifting progressively with decreasing temperature, there appear to be two contributions to the second reduction. As the temperature is lowered by 10 K intervals (Fig. 3), the low temperature component ($E_p^c = -0.53$ V at 223 K) emerges as the other component ($E_p^c = -0.40$ V at 298 K) loses importance, so that at intermediate temperatures both are observed. Lowering the temperature appears to delay the second return wave so that it largely merges with, and enhances, the first return wave. At the lowest temperature, a small return wave at -0.44 V, apparently directly associated with the second reduction, can also be seen. Comparison of these two reduction processes at 223 K by scan rate variation (Fig. 4) was found to mirror the temperature effect, with a progressive decrease in the scan rate rediscovering a shoulder on the return wave of the first reduction process, but without intrusion of the cathodic peak corresponding to the r.t. process (-0.40 V).

The cyclic voltammetric response of the same solution using a switching potential of between -1.80 and -2.00 V (Fig. 5) shows a third non-reversible reduction process which is shifted to more negative potential on lowering the temperature to 223 K. Only a weak, strongly displaced return wave is observed in each case, resulting in a standard potential which is very similar at the two temperatures. The height of the third reduction process is approximately twice the height of the first step, suggesting that the complex can accept four electrons overall in two one-electron and one two-electron reduction processes.

A summary of the voltammetric data is collected in Table 4 and the interpretation of the results shown in Scheme 1. The first two reduction steps correspond to fast, apparently reversible uptake of two electrons at r.t. but the exchange of the second electron becomes more sluggish at lower temperature, causing the associated return wave to be superimposed upon the return wave of the first reduction step. Use of slower scan rates allows a partial recovery of the reversibility of the second process, suggesting that this step may involve a structural change in the complex which is effectively reversible at room temperature, but less so as the temperature is lowered. The third and fourth electrons are added in a single electrochemically irreversible step, regardless of temperature, at a much more negative potential. This may indicate that a substantial structural change accompanies the four-electron acquisition. The displacement of this wave upon cooling is of no particular significance, being simply related to its irreversible nature.

Electrochemical studies of carbonyl clusters have been of interest due to the stability of these complexes in a range of oxidation states, suggesting that they might function as 'electron reservoirs' by allowing the uptake and release of electrons. However, only a few such reports on high-nuclearity clusters have appeared. The reductive electrochemistry of the electron precise decaruthenium anions $[Ru_{10}(\mu\text{-H})(\mu_6\text{-C})(CO)_{24}]^-$ (**3**) and $[Ru_{10}(\mu_6\text{-C})(CO)_{24}]^{2-}$ (**4**) has been reported recently [1]. Two-electron reduction of each complex was found to proceed at significantly more negative potentials than required for **1** ($E_p^c = -0.56$, -0.60 V for **3**, -0.84 V for **4**) and in an electrochemically non- reversible fashion to give $[Ru_{10}(\mu\text{-H})(\mu_6\text{-C})(CO)_{24}]^{3-}$ and $[Ru_{10}(\mu_6\text{-C})(CO)_{24}]^{4-}$, respectively. Spectroelectrochemical studies showed that a structural rearrangement was induced by the reduction process. The structurally altered anions were found to be stable at low temperatures, but they quickly reformed the structurally intact parent complex at higher temperature. A ruthenium–ruthenium bond opening process was postulated. These results are in contrast to studies on the related osmium system, $[Os_{10}(\mu_6\text{-C})(CO)_{24}]^{2-}$, where a fast, reversible one-electron addition was observed followed by a second sluggish, one-electron step. A minor change associated with the second step was seen through spectroelectrochemical studies and proposed to involve cluster vertex expansion [33,34] rather than bond cleavage. The data from the present studies seem

to mimic the osmium system, in that the addition of the second electron involves a sluggish process associated with a structural change which is chemically reversible at r.t. The subsequent addition of a further two electrons in **1** matches the reductive electrochemical behaviour of **3**, where four one-electron reduction steps have been observed [1,35]; interestingly, addition of the third and fourth electrons to **3** ($E_p^c = -1.0, -1.35$ V at r.t.) required less forcing conditions than for **1**, suggesting a further structural change on addition of the four electrons to **1**. Further studies of the structure of both the octa- and deca-ruthenium systems as a function of oxidation level are in progress.

3. Experimental details

$[Ru_3(\mu\text{-H})(\mu\text{-}NC_5H_4)(CO)_{10}]$ was synthesized according to the literature [36]. Chlorodiphenylphosphine (Aldrich) and bis(triphenylphosphoranylidene)ammonium chloride (Aldrich) were used as received. Petrol refers to the fraction with boiling point between 60–80°C. Reactions were carried out using Schlenk techniques [37] under an atmosphere of dry nitrogen; subsequent workup was carried out without any precautions to exclude air.

The IR spectra were recorded using a Perkin-Elmer model 2000 Fourier transform spectrophotometer employing solution cells with CaF_2 windows. Solution NMR spectra were recorded on a Varian Gemini 300 or VXR 300 spectrometer (^{1}H at 300 MHz, ^{31}P at 121 MHz, ^{13}C at 75 MHz). References for the ^{1}H- and ^{13}C-NMR spectra were set to residual solvent peaks. The ^{31}P-NMR proton decoupled solution spectrum was recorded using a recycle delay of 60 s and is reported relative to external 85% H_3PO_4 (0.0 ppm). The solution T_1 measurement was performed using the inversion-recovery technique.

High resolution solid state ^{31}P-NMR experiments were carried out at 162 MHz with a Varian Unity 400 spectrometer, using a high-power amplifier for proton decoupling and a Varian VT probe. Spectra were referenced to external 85% aqueous H_3PO_4 by setting the peak due to external PPh_3 to -10.0 ppm. The kel-F insert, carrying a sample of **1** mixed with KBr, was placed in a silicon nitride rotor with a Torlon end cap and the sample spun at 5000 Hz. A sweep width of 20000 Hz and transmitter offset of 0 Hz were used to observe the region $+65$ to -60 ppm; the proton decoupling strength was approximately 60 kHz, the delay time between successive pulses was 10 s and a contact time of 2 ms was used with cross polarization. Peaks of approximately equal intensity were observed at 6.7 and 9.8 ppm. A sweep width of 60000 Hz and transmitter offset of 100000 Hz were used to observe the region 450 to 800 ppm; no decoupling or cross polarization was applied, and a pulse delay of 900 s was used. A peak was observed at 596.1 ppm.

The mass spectrum was recorded using a VG ZAB 2SEQ instrument (30 kV Cs^+ ions, current 1 mA, accelerating potential 8 kV, 3-nitrobenzyl alcohol matrix) at the Australian National University; peaks were recorded as m/z. Thin layer chromatography was on glass plates (20×20 cm) coated with Merck GF_{254} silica gel (0.5 mm). Electrochemical measurements were recorded using a PAR model 170 system, controlled by a Macintosh LC630 computer and MacLab 4e interface running MacLab EChem software (AD Instruments). Scan rates were typically 100 mV s^{-1} for cyclic voltammetry (CV). Electrochemical solutions contained 0.5 mol dm^{-3} $[NBu^n_4][BF_4]$ and ca. 10^{-3} mol dm^{-3} complex in CH_2Cl_2. The solutions were purged and maintained under an atmosphere of N_2. The jacketted cryostatic glass cell (10 cm^3) contained a platinum disc (0.5 mm diameter) working electrode, platinum auxiliary electrode and Ag–AgCl reference electrode (against which the ferrocene/ferrocenium couple is found at 0.55 V). Measurements were recorded at low temperatures using a Lauda model RL6 cryostat bath to circulate dry MeOH through the cell jacket.

3.1. Preparation of [PPN][$Ru_8(\mu_8\text{-P})(CO)_{22}$]

Chlorodiphenylphosphine (85 μl, 0.47 mmol) was added to a stirred solution of $[Ru_3(\mu\text{-H})(\mu\text{-}NC_5H_4)(CO)_{10}]$ (305 mg, 0.47 mmol) in chlorobenzene (20 ml) and the resultant solution heated at reflux for 40 min. Bis(triphenylphosphoranylidene)ammonium chloride ([PPN]Cl) (204 mg, 0.35 mmol) was then added to the cooled solution, and the mixture stirred for 40 min. The solvent was removed in vacuo, and the red-brown residue purified using thin layer chromatography and a 2:3 acetone in petrol mixture as the eluent. The product from the purple main band ($R_f = 0.6$) was crystallized from CH_2Cl_2/EtOH to afford deep purple crystals of $[PPN][Ru_8(\mu_8\text{-P})(CO)_{22}]$ (**1**, 112 mg, 31%). Anal. Found: C, 34.95; H, 1.19; N, 0.53%; m/z M^- 1456; $C_{58}H_{30}NO_{22}P_3Ru_8$ Calc: C, 34.93; H, 1.51; N, 0.70%; M^- 1456. IR (CH_2Cl_2): ν_{CO} 2049(s), 2024(m), 1985(w), 1790(w) cm^{-1}. ^{1}H-NMR (d_6-acetone): δ 7.73–7.50 (m, PPN). ^{31}P-NMR (CD_2Cl_2, 298 K): δ 774.8 (s, μ_8-P), 620.4 (s, μ_8-P), 21.5 (s, PPN), relative ratios 1: 6.5: 15; (d_6-acetone, 298 K): δ 779.7 (s, μ_8-P), 619.5 (s, μ_8-P), 25.7 (s, PPN); (d_6-acetone, 213 K): δ 784.0 (s, μ_8-P), 631.4 (s, μ_8-P), 25.9 (s, PPN). ^{13}C-NMR (CD_2Cl_2, 298 K): δ 202.8 (m), 201.7 (s) (CO); (CD_2Cl_2, 183 K): δ 202.0 (s), 200.7 (s) (CO). A crystal suitable for the X-ray diffraction study was grown from a CH_2Cl_2/EtOH mixture by slow evaporation of the solvent at r.t.

3.2. X-ray crystallography

A unique r.t. four-circle diffractometer data set was measured ($2\theta/\theta$ scan mode, $2\theta_{max} = 57°$; monochromatic Mo–K_α radiation, $\lambda = 0.71073$ Å; T ca. 295 K) yielding 16087 independent reflections, 12819 with $I > 2\sigma(I)$ being considered 'observed' and used in the large block least squares refinement after gaussian absorption correction. Anisotropic thermal parameter forms were refined for the non-hydrogen atoms; $(x, y, z, U_{iso})_H$ for the cation were included constrained at estimated values. A final difference map was inspected for evidence of cluster bound hydrogen atoms, there being no credible or significant evidence for these ($|\Delta\rho_{max}| = 1.3$ eÅ^{-3}).

Conventional residuals R, Rw at convergence were 0.041, 0.049 [statistical weights, derivative of $\sigma^2(I) = \sigma^2(I_{diff}) + 0.0004\sigma^4(I_{diff})$]. Neutral atom complex scattering factors were employed, computation using the Xtal 3.4 program system [38]. Pertinent results are given in the Figures and Tables, full details of coordinates, thermal parameters, nonhydrogen geometries and structure factor amplitudes being deposited.

Crystal data, $C_{58}H_{30}NO_{22}P_3Ru_8$, $M = 1994.4$, Triclinic, space group $P\bar{1}$ (C_i^1, No. 2), $a = 17.559(6)$, $b = 17.316(4)$, $c = 10.487(3)$ Å, $\alpha = 89.16(2)$, $\beta = 87.68(2)$, $\gamma = 89.07(2)°$, $V = 3185$ Å^3. $D_{calc} = 2.079$ g cm^{-3}; $F(000) = 1916$. $\mu_{Mo} = 19.9$ cm^{-1}; specimen: $0.09 \times 0.48 \times 0.45$ mm; $A^*_{min,\ max} = 1.20,\ 2.15$. $n_v = 831$.

Acknowledgements

We thank the Australian Research Council and the Institute of Advanced Studies (ANU) for support of this work and Johnson-Matthey Technology Centre for the loan of ruthenium salts. MPC holds an ARC Australian Postdoctoral Research Fellowship. MGH is an ARC Australian Research Fellow.

References

[1] M.P. Cifuentes, M.G. Humphrey, G.A. Heath, Inorg. Chim. Acta 259 (1997) 273.
[2] L.J. de Jongh (Ed.), Physics and Chemistry of Metal Cluster Compounds, Kluwer, Dordrecht, 1994.
[3] G. Schmid (Ed.), Clusters and Colloids: From Theory to Applications, VCH, Weinheim, 1994.
[4] M.P. Cifuentes, M.G. Humphrey, in: E.W. Abel, F.G.A. Stone, G. Wilkinson (Eds.), Comprehensive Organometallic Chemistry II, vol. 7, Elsevier, Oxford, 1995, p. 909.
[5] M.P. Cifuentes, M.G. Humphrey, B.W. Skelton, A.H. White, Organometallics 12 (1993) 4272.
[6] M.P. Cifuentes, M.G. Humphrey, B.W. Skelton, A.H. White, J. Organomet. Chem. 507 (1996) 163.
[7] M.P. Cifuentes, M.G. Humphrey, Inorg. Synth. (1997) in press.
[8] M.P. Cifuentes, M.G. Humphrey, A.C. Willis, J. Organomet. Chem. 513 (1996) 85.
[9] M.P. Cifuentes, M.G. Humphrey, B.W. Skelton, A.H. White, Organometallics 14 (1995) 1536.
[10] M.P. Cifuentes, M.G. Humphrey, J.E. McGrady, P.J. Smith, R. Stranger, K.S. Murray, B. Moubaraki, J. Am. Chem. Soc. 119 (1997) 2647.
[11] B.T. Heaton, J.A. Iggo, G. Longoni, S. Mulley, J. Chem. Soc. Dalton Trans. (1995) 1985.
[12] M. Kauppe, J. Chem. Soc. Chem. Commun. (1996) 1141.
[13] D.L. Sunick, P.S. White, C.K. Schauer, Inorg. Chem. 32 (1993) 5665.
[14] P. Chini, G. Ciani, S. Martinengo, A. Sironi, L. Longhetti, B.T. Heaton, J. Chem. Soc. Chem. Commun. 14 (1979) 188.
[15] S.B. Colbran, C.M. Hay, B.F.G. Johnson, F.J. Lahoz, J. Lewis, P.R. Raithby, J. Chem. Soc. Chem. Commun. (1986) 1766.
[16] S.B. Colbran, F.J. Lahoz, P.R. Raithby, J. Lewis, B.F.G. Johnson, C.J. Cardin, J. Chem. Soc. Dalton Trans. (1988) 173.
[17] P. Frediani, M. Bianchi, A. Salvini, F. Piacenti, S. Ianelli, M. Nardelli, J. Chem. Soc. Dalton Trans. (1990) 1705.
[18] P. Frediani, M. Bianchi, A. Salvini, F. Piacenti, S. Ianelli, M. Nardelli, J. Chem. Soc. Dalton Trans. (1990) 165.
[19] F. Van Gastel, N.J. Taylor, A.J. Carty, Inorg. Chem. 28 (1989) 384.
[20] J.L. Vidal, W.E. Walker, R.L. Pruett, R.C. Schoening, Inorg. Chem. 18 (1979) 129.
[21] J.L. Vidal, W.E. Walker, R.C. Schoening, Inorg. Chem. 20 (1981) 238.
[22] J. Mason, J. Am. Chem. Soc. 113 (1991) 24.
[23] J. Mason, J. Am. Chem. Soc. 113 (1991) 6056.
[24] K. Eichele, R.E. Wasylishen, J.F. Corrigan, N.J. Taylor, A.J. Carty, J. Am. Chem. Soc. 117 (1995) 6961.
[25] L.M. Bullock, J.S. Field, R.J. Haines, E. Minshall, D.N. Smit, G.M. Sheldrick, J. Organomet. Chem. 310 (1986) C47.
[26] L.M. Bullock, J.S. Field, R.J. Haines, E. Minshall, M.H. Moore, F. Mulla, D.N. Smit, L.M. Steer, J. Organomet. Chem. 381 (1990) 429.
[27] C.R. Eady, B.F.G. Johnson, J. Lewis, M.C. Malatesta, P. Machin, M. McPartlin, J. Chem. Soc. Chem. Commun. (1976) 945.
[28] G. Ciani, L. Garlascelli, A. Sironi, J. Chem. Soc. Chem. Commun. (1981) 563.
[29] J.L. Vidal, Inorg. Chem. 20 (1981) 243.
[30] V.G. Albano, P. Chini, G. Ciani, M. Sansoni, D. Strumolo, B.T. Heaton, S. Martinengo, J. Am. Chem. Soc. 98 (1978) 5027.
[31] V.G. Albano, P. Chini, G. Ciani, S. Martinengo, M. Sansoni, J. Chem. Soc. Dalton Trans. (1978) 463.
[32] K.M. Mackay, B.K. Nicholson, W.T. Robinson, A.W. Sims, J. Chem. Soc. Chem. Commun. (1984) 1276.
[33] M.H. Barley, S.R. Drake, B.F.G. Johnson, J. Lewis, J. Chem. Soc. Chem. Commun. (1987) 1657.
[34] S.R. Drake, M.H. Barley, B.F.G. Johnson, J. Lewis, Organometallics 7 (1988) 806.
[35] M.P. Cifuentes, M.G. Humphrey, G.A. Heath, unpublished results.
[36] M.I. Bruce, M.G. Humphrey, M.R. Snow, E.R.T. Tiekink, R.C. Wallis, J. Organomet. Chem. 314 (1986) 311.
[37] D.F. Shriver, M.A. Drezdzon, The Manipulation of Air Sensitive Compounds, John Wiley, New York, 1986.
[38] S.R. Hall, G.S.D. King, J.M. Stewart (Eds.), The XTAL 3.4 Reference Manual, University of Western Australia, Lamb Press, Perth, 1995.